Experimental evidence for lava-like mud flows under Martian surface conditions

Petr Brož, Ondřej Krýza, Lionel Wilson, Susan J. Conway, Ernst Hauber, Adriano Mazzini, Jan Raack, Matthew R. Balme, Matthew E. Sylvest, Manish R. Patel

Experimental evidence for lava-like mud flows under Martian surface conditions

Petr Brož[1*], Ondřej Krýza[1], Lionel Wilson[2], Susan J. Conway[3], Ernst Hauber[4], Adriano Mazzini[5], Jan Raack[6], Matthew R. Balme[7], Matthew E. Sylvest[7] and Manish R. Patel[7,8]

[1]Institute of Geophysics of the Czech Academy of Sciences, Boční II/1401, 141 31, Prague, Czech Republic

[2] Lancaster Environment Centre, Lancaster University, Lancaster LA1 4YQ, UK

[3] CNRS UMR-6112 LPG Nantes, France

[4]Institute of Planetary Research, DLR, Rutherfordstr. 2, 12489, Berlin, Germany

[5]Centre for Earth Evolution and Dynamics (CEED), University of Oslo, Norway

[6]Institut für Planetologie, Westfälische Wilhelms-Universität Münster, Germany

[7]School of Physical Science, STEM, The Open University, Milton Keynes, UK Open University, Milton Keynes, United Kingdom

[8]Space Science and Technology Department, STFC Rutherford Appleton Laboratory, Oxford, UK

Corresponding Author

Petr Brož

Institute of Geophysics of the Czech Academy of Sciences

Boční II/1401

14131 Prague 4

Czech Republic

Petr.broz@ig.cas.cz

+420267103063

Large outflow channels on ancient terrains of Mars have been interpreted as the products of catastrophic flood events. The rapid burial of water-rich sediments following such flooding could have led to sedimentary volcanism, in which mixtures of sediment and water (mud) erupt to the surface. Tens of thousands of volcano-like landforms populate the northern lowlands and other local sedimentary depocenters on Mars. However, it is difficult to determine whether the edifices are related to igneous or mud extrusions, partly because the behaviour of extruded mud under martian surface conditions is poorly constrained. Here, we investigate the mechanisms of mud propagation on Mars using experiments performed inside a low-pressure chamber at cold temperatures. We find that low viscosity mud under martian conditions propagates differently from on Earth, because of rapid freezing and the formation of an icy crust. Instead, the experimental mud flows propagate like terrestrial pahoehoe lava flows, with liquid mud spilling from ruptures in the frozen crust, then refreezing to form a new flow lobe. We suggest that mud volcanism can explain the formation of some lava-like flow morphologies on Mars, and that similar processes may apply to cryovolcanic extrusions on icy bodies in the Solar System.

The physics behind igneous volcanism on Mars is better understood [e.g., 1-4] than that of sedimentary volcanism in which mixtures of water and sediment, subsequently referred to as mud, are extruded onto the surface. On Earth, sedimentary volcanism manifests at the surface as eruptions of fluids (water, gas, occasionally oil), fine grained sediments (e.g. clays) and clasts from the country-rock. These geological phenomena are the result of fluid (on Earth typically associated with methane) overpressure [5], generated at several hundred to several thousand metres depth, combined with gravitational instability of buoyant sedimentary units buried at deeper stratigraphic levels [6]. The viscosity of ascending mud varies, and affects the shapes, sizes and thicknesses of resulting flows. The higher the water

content, the lower the viscosity and vice versa (Figure 1). The focus of our experimental investigation are water-dominated mud flows that propagate over shallow slopes via centimetre-thick flows (Fig. 1a,b), as opposed to clay-dominated flows that can be meter(s) thick (Fig. 1c).

Although the propagation of water at low atmospheric pressure has been previously studied [7-11], there is a lack of theoretical and empirical knowledge about the behaviour of mud at low atmospheric pressure, temperature and gravity, despite an initial study by [12]. This knowledge gap represents an obstacle in the study of landforms interpreted to be the result of mud extrusion on Mars [13-24] and other terrestrial or icy solar system bodies. Currently, the low martian atmospheric pressure inhibits the sustained presence of liquid water on the surface [e.g., 7-11,25,26], so evaporation and ice-formation cause the rheology of the extruded mud to change rapidly; hence mud flows could propagate differently from on Earth [17].

We used analogue experiments performed in a low pressure chamber to examine how low viscosity, water-dominated mud with a solid fraction of less than ~6.5 wt.% (12.7 mPa.s at 276 K and 10.7 mPa.s at 296 K) propagates over a cold surface (244 K to 265 K) under terrestrial and martian (7 mbar) atmospheric pressures. These experiments enabled comparing flow mechanisms at different pressures to be compared and reveal a unique propagation behaviours under martian conditions. Based on these observations we propose that evaporation and surficial freezing would dominate the morphology for relatively thin mud flows (< 1 m) and may influence thicker mud flows hypothesized to be present on the martian surface [e.g. 12,15,17,24,25].

Mud flow experiments

We performed 21 experiments (Table S1 and Fig. S1 in Supplementary Information) using the Open University (UK) Mars Chamber. During each experiment, 500 ml of mud was poured over a 0.9 × 0.4 m aluminium tray containing either (a) a ~2 cm deep sand bed (~63–200 μm grain diameter; 14 experiments) representing a sedimentary surface, or (b) a plastic plate (7 experiments) representing an impermeable icy surface. Fifteen experiments were performed at 7 ± 0.5 mbar and six experiments at ~1 bar (Table S1). The mud was released onto the surface from a tilting container situated inside the chamber. This design was chosen for its simplicity and reproducibility, although it represents a simplification of the natural setting. At the beginning of the experiment the mud was above the freezing point of water. The temperatures of the sand bed or plastic plate ranged from ~244 K to 265 K and gradually increased with time as no active cooling of the experiment was performed. The aluminium tray was inclined at 5° (18 experiments) or 10° (3 experiments) to force the mud to move in a preferred direction. Each experimental run was performed at least in triplicate and was recorded with four cameras. The experiments did not account for the effect of the lower gravity on Mars as compared to Earth.

At the beginning of each experiment the atmospheric pressure was gradually reduced, triggering the boiling of the water in the mud [25,27,28]. The mud within the container cooled by evaporation [25] to almost its freezing point before being poured onto the surface at a pressure of 7 ± 0.5 mbar (Table S1). Once in contact with the cold surface, the mud rapidly began to freeze at the bottom and margins of the flow, and at its upper surface (Fig. 2a and Supplementary Information). The freezing resulted in the formation of an ice-mud crust which modified flow propagation and decreased lateral spreading (Fig. 3).

Mud propagation occurred through an intricate system of narrow flow lobes (Fig. 3b) or several lobate flows (Fig. 3c and 3d). Their formation was controlled by the development of frozen marginal ridges that confined the flow of liquid mud inside a central channel. As

freezing continued, ice crystals floated to the surface and started to merge. However, mud still propagated within the crust via a network of "mud tubes", in an analogous way to flow within lava tubes (Fig. 2c). When new pulses of mud arrived, they caused breakouts and the formation of further lobes (Fig. 2b). The newly extruded material rapidly developed a frozen crust.

The presence of internal mud tubes was confirmed by sectioning the frozen mud flows after the re-pressurization of the chamber. A liquid mud core was present even in the experiments where mud was exposed to low pressure for several tens of minutes (Fig. 2d,e). Vesicles ranging in size from 1 to 10 mm were observed within the crusts (Fig. 2d), produced by vapour bubbles that did not escape. The vesicular nature of the crust inhibited the conduction of heat [29] from the interior of the flow, increasing the depth to which vapour bubble nucleation occurred.

Comparison with terrestrial lava flows

During flow formation, newly supplied mud was observed to increase the thickness of lobes up to several centimetres (Fig. 3d) via lifting of the protective crust. This occurred when the terminal part of the flow was frozen and the mud release was blocked, but newly supplied mud was still intruding the lobe via mud tubes. This created overpressure within the mud which was able to lift the crust of the lobes. Once a sufficient volume of mud had accumulated within the lobe, the overpressure was able to break the crust and a new lobe formed at the terminus. The mud flow inflated in a manner directly analogous to that of pahoehoe lava flows [30]. This inflation was observed on 5° and 10° slopes, and for impermeable and permeable substrates. Under terrestrial atmospheric conditions (i.e. room pressure and temperature) a mud flow moving over a cold surface did not form lobes, did not inflate, and had no icy crust (Fig. 3d) regardless of the temperature of the mud (~274, ~290, and ~293 K were tested). Instead, the mud spread out over the surface in a broad sheet

only a few millimetres thick, and was in the liquid phase over the entire length of the flow (Fig. 3a,d). Only minor freezing was observed in the form of ice crystals on the margins of the flow after several minutes.

Like basaltic lavas on Earth, low viscosity mud flows produce laterally extensive structures with lower relief than those resulting from high viscosity flows [6]. Because the mud used in our experiments is water-dominated, it initially behaves as a Newtonian fluid. In the low-pressure environment, evaporative cooling leads to the formation of ice crystals, which increase the solid content forming a protective crust. The mud evolves into a non-Newtonian fluid with non-zero yield strength as the total solid volume fraction increased beyond ~15% [31]. This behaviour is similar to that of low viscosity basaltic lavas whose movement is affected by the formation of an external crust, formed by solidification of the lava due to cooling [32]. In both cases the strength of the visco-elastic part of the crust, between the brittle outer part and the more fluid interior [30], is able to inhibit lateral spreading and allows fluid accumulation and vertical inflation.

Over time, the water in the flow (i.e. not lost by evaporation) freezes to form ice in the crust, and hence, the thin crust develops an ever-increasing yield strength due to the ice crystal network becoming increasingly interconnected between the clay particles (see rheology references in [33]). This creates a solid with mechanical strength similar to how mineral crystal frameworks in a cooling silicate rock magma replace the rheological yield strength of the lava. Thus the strength of the crust increases with time, and more inflation should occur before breakouts occur, in agreement with our observation of more inflation in the distal parts of the experimental flows. There is no reason to assume that the mechanical strength of the crust would be different on Mars for mud with the same clay content. Since the rate, as well as the mode, of its formation are controlled by the non-equilibrium thermodynamics of vapour loss, specifically the transfer of sensible heat to latent heat in the

liquid surrounding each nucleating vapour bubble [25], the time-scale of crust development should also be the same on Mars. Calculations describing these processes are reported in the Supplementary Information.

The above arguments assume that, as in the experiments, the motion of the mud is laminar. However, it is likely that in large flows, that the fluid motion is turbulent. For steady, uniform laminar flows of mud with viscosities of 0.01, 0.1, 1 and 10 Pa.s on 0.6° slopes under martian gravity, the transition to turbulence will occur for mud flows with thicknesses of 17 mm, 8 cm, 36 cm and 1.7 m, respectively (see equations in [12]). As the solid content (silicate particles and ice crystals) of the mud increases, its viscosity increases, but even for a total solids content of 60% [e.g. 34] the viscosity does not exceed 1 Pa.s. Thus any low viscosity mud flow thicker than a few tens of centimetres on Mars will probably be turbulent and we discuss the applicability of our experiments to this case below.

Implications for mud flows on planetary surfaces

In a model of mud flow dynamics on Mars, [12] considered the effect of high solid content on the non-Newtonian rheology of mud, assuming the rheological properties were constant everywhere along the flow. Our experiments underline the importance of considering the thermodynamics of the processes that occur when mud is exposed to the martian environment. In a turbulent mud flow, mud from all depths will be exposed to the low atmospheric pressure and will boil, lose vapour, and cool. Thus, it will cool rapidly, increasing the ice crystal content and evolving a yield strength. As the yield strength increases, the critical Reynolds number required to sustain turbulence increases [35], but the associated increase in viscosity causes the actual Reynolds number to decrease. When the two become equal this forces a transition to laminar flow, encouraging the formation of lobes and breakouts, as observed in our experiments.

Although our small-scale experimental mudflows show characteristics similar to those of low-viscosity lava flows, they have a different heat loss mechanism. For lava flows simulated in the laboratory using wax [e.g., 36-37] a modified Péclet number has been used to distinguish flows that do or do not readily form crusts. This is not appropriate for our flows, where the heat loss mechanism is decompressional boiling, not conduction and convection into the environment (for details see Supplementary Information).

On Earth, low effusion rates and volumes can lead to the formation of mud flows (Fig. 1a,b) with similar magnitudes to those in our experiments. Therefore, such terrestrial flows exported to Mars would be strongly affected by the mechanisms observed in our experiments. We expect these mechanisms to also be important at the margins of kilometre-scale flows where their thicknesses decreases and numerous overlapping centimetre-thick flows occur. Once mud is extruded into the martian surface pressure environment, it would cool due to evaporative cooling (Fig. 4a) and freezing of the flow surface would eventually cause a change in the flow regime. From that point, the mud would no longer propagate via open channel(s) (Fig. 4b), but instead via mud tube(s) (Fig. 4c) and lobes (Fig. 4d). The distance such a transition occurs from the source would depend on the effusion rates, volumes, viscosity and temperature of the extruded mud.

Our study shows that inflation of decimetre-thick and meter-sized lobes could occur at the margins of both mud flows and lava flows, thus both igneous and mud volcanism surface flows could have similar morphological characteristics [e.g., 12,17]. Our calculations show that the morphologies of mud flows at scales larger than those covered by our experiments could be affected by the same processes, particularly at their margins. Hence, as their mechanisms of mud propagation would differ, martian mud volcanoes may be substantially different in shape from terrestrial ones [17].

Sedimentary volcanism has also been proposed for the dwarf planet Ceres [38,39], which may have a water-muddy ocean beneath a crust made of clays, salts, clathrates and ice [39,40]. The process of evaporative cooling and associated freezing should also occur there, affecting the morphologies of resulting effusive landforms; even more so on Ceres than on Mars as Ceres lacks an atmosphere. The same principles would apply to other Solar System bodies and icy moons, and so our experimental results should be considered when interpreting effusive cryovolcanic surface features on these bodies [e.g., 41,42]. Our results show that it is vital to consider the effects of the differing environmental conditions on other planetary surfaces when comparing analogue landforms observed on Earth with apparently similar effusive morphologies on other bodies.

References

[1] Wilson, L., & Head, J. W. Mars: Review and analysis of volcanic eruption theory and relationships to observed landforms. Reviews of Geophysics 32(3), 221–263 (1994). https://doi.org/10.1029/94RG01113

[2] Brož, P., Čadek, O., Hauber, E., & Rossi, A. P. Scoria cones on Mars: Detailed investigation of morphometry based on high-resolution digital elevation models. Journal of Geophysical Research: Planets 120, 1512–1527 (2015). https://doi.org/10.1002/2015JE004873

[3] Parfitt, E. A., & Wilson L. Fundamentals of Physical Volcanology (Blackwell, Oxford, U. K., 2008). ISBN: 978-0-632-05443-5

[4] Fagents, S. A, Gregg, T. K. P., & Lopes, R. M. C. Modelling volcanic processes: the physics and mathematics of volcanism (Cambridge University Press, Cambridge, 2013). ISBN: 9781139021562

[5] Dimitrov, L. I. Mud volcanoes—the most important pathway for degassing deeply buried sediments. Earth-Science Reviews 59, 1–4, 49–76 (2002). https://doi.org/10.1016/S0012-8252(02)00069-7

[6] Mazzini, A., & Etiope, G. Mud volcanism: An updated review. Earth-Science Reviews 168, 81–112 (2017). https://doi.org/10.1016/j. earscirev.2017.03.001

[7] Wallace, D., & Sagan, C. Evaporation of ice in planetary atmospheres: Ice-covered rivers on Mars. Icarus 39, 385–400 (1979). https://doi.org/10.1016/0019-1035(79)90148-9

[8] Carr, M. H. Stability of streams and lakes on Mars. Icarus 56, 476–495 (1983). https://doi.org/10.1016/0019-1035(83)90168-9

[9] Baker, V. R. Erosional processes in channelized water flows on Mars. Journal of Geophysical Research 84, 7985–7993 (1979). https://doi.org/10.1029/JB084iB14p07985

[10] Brass, G.W. The stability of brines on Mars. Icarus 42, 20–28 (1980). https://doi.org/10.1016/0019-1035(80)90237-7

[11] Kossacki, K. J., Markiewicz, W. J., Smith, M. D., Page, D., & Murray, J. Possible remnants of a frozen mud lake in southern Elysium, Mars. Icarus 181, 363–374 (2006). https://doi.org/10.1016/j.icarus.2005.11.018

[12] Wilson, L., & Mouginis-Mark, P. J. Dynamics of a fluid flow on Mars: Lava or mud? Icarus 233, 268–280 (2014). https://doi.org/10.1016/j.icarus.2014.01.041

[13] Oehler, D.Z. & Allen, C.C. Evidence for pervasive mud volcanism in Acidalia Planitia, Mars. Icarus 208, 636–657 (2010). https://doi.org/10.1016/j.icarus.2010.03.031

[14] Allen, C.C. et al. Fluid expulsion in terrestrial sedimentary basins: a process providing potential analogs for giant polygons and mounds in the martian lowlands. Icarus 224, 424–432 (2013). https://doi.org/10.1016/j.icarus.2012.09.018

[15] Komatsu, G. et al. Small edifice features in Chryse Planitia, Mars: Assessment of a mud volcano hypothesis. Icarus 268, 56–75 (2016). https://doi.org/10.1016/j.icarus.2015.12.032

[16] Hemmi, R., & Miyamoto, H. High-resolution topographic analyses of mounds in southern Acidalia Planitia, Mars: Implications for possible mud volcanism in submarine and subaerial environments. Geosciences, 8(5), 152, 1–19 (2018). https://doi.org/10.3390/geosciences8050152

[17] Brož, P., Hauber, E., van de Burgt, I., Špillar, V., & Michael, G. Subsurface sediment mobilization in the southern Chryse Planitia on Mars. Journal of Geophysical Research: Planets 124, 703–720 (2019). https://doi.org/10.1029/2018JE005868

[18] Okubo, C. H. Morphologic evidence of subsurface sediment mobilization and mud volcanism in candor and Coprates Chasmata, Valles Marineris, Mars. Icarus 269, 23–37 (2016). https://doi.org/10.1016/j.icarus.2015.12.051

[19] Skinner, J. A., & Mazzini, A. Martian mud volcanism: Terrestrial analogs and implications for formational scenarios. Marine and Petroleum Geology 26(9), 1866–1878 (2009). https://doi.org/10.1016/j.marpetgeo.2009.02.006

[20] Hemmi, R. & Miyamoto, H. Distribution, morphology, and morphometry of circular mounds in the elongated basin of northern terra sirenum, mars. Progress in Earth and Planetary Science 4, 26, 1–15 (2017). https://doi.org/10.1186/s40645-017-0141-x

[21] Kumar, P. S. et al. Recent seismicity in Valles Marineris, Mars: Insights from young faults, landslides, boulder falls and possible mud volcanoes, Earth and Planetary Science Letters 505, 51–64 (2019). https://doi.org/10.1016/j.epsl.2018.10.008

[22] Brož, P., & Hauber, E. Hydrovolcanic tuff rings and cones as indicators for phreatomagmatic explosive eruptions on Mars. Journal of Geophysical Research: Planets 118, 1656–1675 (2013). https://doi.org/10.1002/jgre.20120

[23] Brož, P., Hauber, E., Wray, J. J., & Michael, G. Amazonian volcanism inside Valles Marineris on Mars. Earth and Planetary Science Letters 473, 122–130 (2017). https://doi.org/10.1016/j.epsl.2017.06.003

[24] Skinner, J. A., & Tanaka, K. L. Evidence for and implications of sedimentary diapirism and mud volcanism in the southern Utopia highland-lowland boundary plain, Mars. Icarus 186(1), 41–59 (2007). https://doi.org/10.1016/j.icarus.2006.08.013

[25] Bargery, A. S., Lane, S. J., Barrett, A., Wilson, L., & Gilbert, J. S. The initial responses of hot liquid water released under low atmospheric pressures: Experimental insights. Icarus 210(1), 488–506 (2010). https://doi.org/10.1016/j.icarus.2010.06.019

[26] Hecht, M. H. Metastability of liquid water on Mars. Icarus 156(2), 373–386 (2002). https://doi.org/10.1006/icar.2001.6794

[27] Raack, J. et al. Water-induced sediment levitation enhances downslope transport on Mars. Nature Communications 8, 1–10 (2017). https://doi.org/10.1038/s41467-017-01213-z

[28] Herny, C. et al. Downslope sediment transport by boiling liquid water under Mars-like conditions: Experiments and potential implications for Martian gullies. Geological Society Special Publication 467, 373-410 (2019). https://doi.org/10.1144/SP467.10

[29] Smith, D. et al. Thermal conductivity of porous materials. Journal of Materials Research 28(17), 2260–2272 (2013). https://doi.org/10.1557/jmr.2013.179

[30] Hon, K., Kauahikaua, J., Denlinger, R., & Mackay, K. Emplacement and inflation of pahoehoe sheet flows: observation and measurements of active lava flows on Kilauea

285 Volcano, Hawaii. Geological Society of America Bulletin 106, 351–370 (1994).
286 https://doi.org/10.1130/0016-7606(1994)106<0351:EAIOPS>2.3.CO;2

287 [31] Ayel, V., Lottin, O., & Peerhossaini, H. Rheology, flow behaviour and heat transfer of ice
288 slurries: a review of the state of the art. International Journal of Refrigeration 26, 95–107
289 (2003). https://doi.org/10.1016/S0140-7007(02)00016-6

290 [32] Cashman, K. V., Kerr, R. C., & Griffiths, R. W. A laboratory model of surface crust
291 formation and disruption on lava flows through non-uniform channels. Bulletin of
292 Volcanology 68(7-8), 753–770 (2006). https://doi.org/10.1007/s00445-005-0048-z

293 [33] Chevrel M. O., Baratoux, D., Hess, K.-U., & Dingwell, D. B. Viscous flow behavior of
294 tholeiitic and alkaline Fe-rich martian basalts. Geochimica et Cosmochimica Acta 124,
295 348–365 (2014). https://doi.org/10.1016/j.gca.2013.08.026

296 [34] Kaitna, R., Rickenmann, D. & Schatzmann, M., Experimental study on rheologic
297 behaviour of debris flow material. Acta Geotechnica 2, 71–85 (2007).
298 https://doi.org/10.1007/s11440-007-0026-z

299 [35] Skelland, A.H.P. Non-Newtonian flow and heat transfer. (John Wiley and Sons, New
300 York, 1967).

301 [36] Rader, E., Vanderkluysen, L., & Clarke, A. The role of unsteady effusion rates on
302 inflation in long-lived lava flow fields. Earth and Planetary Science Letters 477, 73–
303 83 (2017). https://doi.org/10.1016/j.epsl.2017.08.016

304 [37] Fink, J. H., & Griffiths, R. W. A laboratory analog study of the morphology of lava
305 flows extruded from point and line sources. Journal of Volcanology and Geothermal
306 Research 54, 19–32 (1992). https://doi.org/10.1016/0377-0273(92)90112-Q

[38] Sori, M. M. et al. The vanishing cryovolcanoes of Ceres. Geophysical Research Letters 44, 1243–1250 (2017). https://doi.org/10.1002/2016GL072319

[39] Ruesch, O. et al. Slurry extrusion on Ceres from a convective mud-bearing mantle. Nature Geoscience 12, 505–509 (2019). https://doi.org/10.1038/s41561-019-0378-7.

[40] Marchi, S. et al. An aqueously altered carbon-rich Ceres. Nature Astronomy 3, 140–145 (2018). https://doi.org/10.1038/s41550-018-0656-0.

[41] Allison, M. L. & Clifford, S. M. Ice-covered water volcanism on Ganymede. Journal of Geophysical Research 92, 7865–7876 (1987). https://doi.org/10.1029/JB092iB08p07865

[42] Fagents, S.A. Considerations for effusive cryovolcanism on Europa: The post-Galileo perspective. Journal of Geophysical Research: Planets 108 (E12), 5139 (2003). https://doi.org/10.1029/2003JE002128

Acknowledgements

The access to the Mars Chamber at the Open University was provided by Europlanet 2020 RI which has received funding from the European Union's Horizon 2020 research and innovation program under grant agreement No 654208. OK was supported by Center for Geosphere Dynamics (Faculty of Science at Charles University) project UNCE/SCI/006. LW was supported by the Leverhulme Trust through an Emeritus Fellowship. AM received funds from the European Research Council under the European Union’s Seventh Framework Programme Grant agreement n° 308126 (LUSI LAB project, PI A. Mazzini) and acknowledges the support from the Research Council of Norway through its Centres of Excellence funding scheme, Project Number 223272 (CEED). The authors thank Steve Lane and Ondřej Čadek for valuable discussions, Rudolf Koranda from Keramost Company for providing the clay samples, and to Laszlo Keszthelyi and Alison Graettinger for their constructive comments and insightful suggestions, which significantly improved this manuscript.

Author contribution

The experimental set-up and the methodology were conceived and designed by P.B. and O.K. with the help and advice of S.J.C., J.R., M.R.P., M.R.B., A.M., and E.H. The technical support was provided by M.R.S. The data analysis was done by P.B. with significant feedback from O.K., L.W., S.J.C., E.H. and A.M. The DEM production was done by O.K. and the theoretical considerations associated with scaling were done by L.W. All authors contributed to discussion, interpretation and writing of the manuscript.

Competing interests

The authors declare no competing interests.

Figure captions

Fig. 1. **Examples of surface expressions of terrestrial sedimentary volcanism caused by muds of various viscosity**. (a) A water-dominated mud flowing from the crater of Bakhar mud volcano in Azerbaijan (39°59'55.7"N, 49°28'29.9"E). (b) An individual mud flow from a 'gryphon' on top of Dashgil volcano in Azerbaijan (39°59′48″N, 49°24′11″E). (b). (c) A kilometre-sized highly-viscous mud flow outgoing from Koturdag mud volcano in Azerbaijan (39°58′30″N, 49°21′36″E). Note minibus for scale.

Fig. 2. **Examples of morphologies and interior structures of mud flows formed in a low-pressure environment**. Panel **a** shows three frames from video taken by Cam #2 covering experiment #16 in which the formation of a narrow, thick mud flow occurred. Panel **b** shows in detail the formation of the icy crust and outbreaks of new mud pulses from beneath the icy-muddy crust. When the resulting mud flow features were sectioned, large cavities filled with liquid mud (**c**), or voids (**d**) in the ice were observed. A liquid mud core was commonly observed in the flow interior (**e**).

Fig. 3. **Timeline maps of modelled mud flows derived from the videos and final topographic cross sections**. Flows formed in terrestrial (**a**) and low-pressure environments when mud was poured by high (**b**) or low (**c**) release rates. The numbered bold lines represent the margins of the flows at 5 s intervals, the other lines are 1 s intervals. (**d**) The position of each topographic profile is marked in panels **a**, **b** and **c**. Topography was measured after the chamber was re-pressurized.

Fig. 4. **Hypothesised development of a low viscosity mud flow on Mars.** (**a**) The mud boils and self-cools through evaporative cooling. Once a mud flow develops, the mud is transported via an open channel (**b**) evolving into a mud tube due to freezing of the flow surface (**c**). The mud propagates via mud tubes to the flow front. As the crust prevents free movement of the mud, it spreads via lobe breakout (**d**) which occurs when the pressure inside the frozen flow is large enough to break the crust or to lift it up; exposing the mud again to the martian environment.

Methods

Experimental setup. The low viscosity mud used in our experiments was a mixture of water that contains 0.5 % w/w dissolved magnesium sulphate ($MgSO_4$) salts corresponding to the average river water salinity and clay obtained from the claystone named after the Rokle locality operated by the company Keramost, which is situated near the town of Kadaň in the Czech Republic. The clay was a bentonite composed of 76 % montmorillonite, 23 % illite, and 1 % kaolinite which has been formed by alteration of pyroclastic rocks. As there is no direct in-situ knowledge of which types of clays could be present on Mars during subsurface sediment mobilization and as explosive volcanism was once present on Mars [42], to the first approximation this material seems to be a suitable analogue. To exclude the presence of potentially more lithified clayey aggregates, the clay was mixed with water and salt and homogenized in a blender for 3 minutes. Adding the small amount of the salt was necessary to

allow submillimetre particles to get into suspension within the mixture [43] and also realistic for the martian surface [e.g., 44-46]. The resulting viscosity of the mud was 12.7 mPa.s at ~276 K and 10.7 mPa.s at ~296 K and the average density of the mixture was 1037.5 $kg.m^{-3}$. The viscosity was measured with Haake Rotovisco RV 20 and Viscotester VT 550 rheometers (Institute of Hydrodynamics of the Czech Academy of Sciences) with ledges on the MV2 cylinder to prevent slip of the measured material on its walls.

Each experimental run (for details see Table S1 in the Supplementary Information) started by inserting the 0.9 × 0.4 m aluminium tray filled with (a) a ~2 cm deep substrate bed (natural sand, ~200 μm), or b) a plastic plate, and similarly sized copper plate inside the freezer to pre-cool the tray and the plate to temperatures around 238 K. Once the required temperature was reached, the plate and the tray were inserted inside the vacuum chamber. At the same time the 500 ml of liquid mud was poured inside the tilting container equipped with one thermocouple to record the temperature of the mud, and the container was installed inside the chamber. The temperature of the mud varied from 274 to 297 K before the pressure drop. The temperature within the chamber was also monitored by another thermocouple. Additionally, five thermocouples were set in a grid (see Fig. 1 in the Supplementary Information for details about the positioning of thermocouples) within the tray in order to monitor the temperature of the surface over which the mud propagated.

Once the tray was in place inside the chamber, a series of images were taken by a single-lens reflex camera from different angles to obtain the digital elevation model of the pristine surface before the experimental ran. Subsequently the chamber was closed and the process of depressurization started. To achieve the pressure drop from ambient terrestrial pressure to 7 mbar took usually around 6 minutes. Once the pressure started to drop, the decrease in the temperature of the mud within the container was measured. Every time the mud self-cooled close to 273 K during the pressure drop, but it remained liquid. When the pressure of ~7 mbar

was reached, the container was manually flipped by the operator and hence mud was poured from the height of ~5 cm to the surface. The mud flux was not directly measured, we recorded only the time for how long the mud was extruded (Table S1), as the intense boiling occurred within the container and hence caused irregularities within the flux.

The movement of the mud over the surface was recorded by four video cameras. Once the mud propagation stopped, the resulting mud flow feature was left in the low pressure environment for various lengths of time ranging from several minutes to about one hour. After that the process of re-pressurization of the chamber to terrestrial values started, typically before temperature of the tray surface rose above ~273 K. Once the pressure inside the chamber reached atmospheric pressure, the chamber was opened and the resulting flow features were documented by taking images from different angles to acquire data for subsequent DEM production. Ultimately the mud flows produced were sectioned and their inner structure was investigated and documented.

DEM production. To compare the elevation profiles along and perpendicular to the flow directions of the mud flows we calculated a series of digital elevation models (DEM). The sedimentary bed was photographed after each experimental procedure ~30-70 times from multiple viewpoints. The reconstruction of a 3D model surface was produced by using the 'Structure-from-Motion' [47] commercial software Agisoft PhotoScan. For image orientation correlation and scaling of the 3D models we used twelve fixed black-on-white printed markers which were affixed onto flat topped cylindrical posts. The posts had two different elevations (4.6 cm and 9.6 cm) and the markers were ~2.67 cm in diameter. Typical discrepancies between actual and calculated marker positions were ~0.8 - 1.6 mm. Exported DEMs and orthophotos (TIFF format) were imported to QGIS for further analysis and production of the elevation profiles.

Cooling and freezing of mud when the external pressure is less than the saturation vapour pressure of the water. Both the silicate component and the water that has not yet vaporized will cool from the initial temperature until the freezing point is reached. After the freezing point is reached, the temperature remains constant and vapour continues to be lost until all of the remaining water has been converted to ice. If the external pressure is less than the saturation vapour pressure of the ice, evaporation continues, the frozen mud surface cools, and a wave of cooling propagates into the frozen mud. The bulk density of the mud changes continuously throughout these stages as a function of the initial mass fractions of silicate and water in the mud. Let the initial masses of water and silicate in a given sample of the mud be m_w and m_s, respectively, the volumes of water and solid be v_w and v_s, respectively, and the corresponding densities be ρ_w and ρ_s. Let the bulk density of the mud be β. Then

$$\beta = (m_w + m_s) / (v_w + v_s) = (m_w + m_s) / [(m_w / \rho_w) + (m_s / \rho_s)] \quad (1).$$

Expanding, collecting terms and simplifying:

$$m_w / m_s = (\rho_w / \rho_s) [(\rho_s - \beta) / (\beta - \rho_w)] \quad (2).$$

We next find the mass of vapour, M_{vc}, that must be lost from the water to cool the remaining water and silicate to any given lower temperature. Let the initial mud temperature be θ_i and the final temperature be θ_f. The heat H_v removed from the water by the formation of the vapour is

$$H_v = M_{vc} L_v \quad (3)$$

where L_v is the latent heat of vapourization, 2.46×10^6 J kg^{-1}. During this cooling process, the liquid water mass decreases from its initial value m_w to a smaller final value m_f, where by definition

$$m_f = m_w - M_{vc} \quad (4).$$

Thus, the average mass of water, m_a, during the cooling process is

$$m_a = 0.5\,(m_w + m_f) = 0.5\,(m_w + m_w - M_{vc}) = (m_w - 0.5\,M_{vc}) \quad (5).$$

As long as the specific heat of the water can be approximated as a constant, the heat the water loses while cooling is H_c where

$$H_c = m_a\,C_w\,(\theta_i - \theta_f) \quad (6)$$

and C_w is the specific heat of water, 4186 J kg^{-1} K^{-1}. The silicate mass m_s also cools, and loses an amount of heat equal to H_s where

$$H_s = m_s\,C_s\,(\theta_i - \theta_f) \quad (7).$$

Here C_s is the specific heat of the silicate, say 1000 J kg^{-1} K^{-1}. Equating the sum of H_c and H_s to H_v,

$$(m_w - 0.5\,M_{vc})\,C_w\,(\theta_i - \theta_f) + m_s\,C_s\,(\theta_i - \theta_f) = M_{vc}\,H_v \quad (8)$$

and regrouping,

$$M_{vc} [H_v + 0.5 C_w (\theta_i - \theta_f)] = (m_w C_w + m_s C_s) (\theta_i - \theta_f) \quad (9)$$

or

$$M_{vc} / m_s = \{[(m_w /m_s) C_w + C_s] (\theta_i - \theta_f)\} / [H_v + 0.5 C_w (\theta_i - \theta_f)] \quad (10).$$

Using equation (2) for (m_w / m_s) we can also find (M_{vc} / m_s) as a function of the assumed value of ρ_s. Finally, the ratio, R, of the mass of water converted to vapour to the initial water mass, i.e. $R = (M_{vc} / m_w)$, is equal to $[(M_{vc} / m_s) (m_s / m_w)]$ or more conveniently

$$R = [(M_{vc} / m_s) / (m_w / m_s)] \quad (11).$$

The mass of water remaining in the mud after the cooling phase, m_f, is therefore

$$m_f = (1 - R) m_w \quad (12).$$

The above equations apply between any pair of temperatures θ_i and θ_f until θ_f becomes equal to the freezing point, θ_{fr}. After the freezing point is reached, the temperature remains constant while liquid water continues to evaporate and the latent heat of vaporization is extracted from the remaining water, progressively freezing into ice all of the water that is not lost as vapour. The latent heat of vaporization in the 283-293 Kelvin range is 2.46×10^6 J kg^{-1} and the latent heat of solidification is 3.34×10^5 J kg^{-1}. The ratio of these is $Q = (3.34 \times 10^5 / 2.46 \times 10^6) = 0.13577$. Thus, to produce 1 kg of ice we would have to evaporate 0.13577 kg of

503 water into vapour from an initial total mass of 1.13577 kg of water. A fraction [Q/(1 + Q)] of
504 the water mass remaining after cooling must become vapour and a fraction [1/(1 + Q)] of the
505 water mass remaining after cooling becomes ice. The final ice mass, m_i, is
506
507 $$m_i = [1/(1 + Q)]\ [(1 - R)\ m_w] \quad (13)$$
508
509 and the mass of water converted to vapour during the freezing phase is M_{vf} where
510
511 $$M_{vf} = [Q/(1 + Q)]\ (1 - R)\ m_w \quad (14).$$
512
513 The total mass of vapour generated by the whole process is $M_v = M_{vc} + M_{vf}$.
514
515 As a result of the loss of vapour, the bulk density of the frozen mud will be different from
516 the density of the initial mixture. The ice has a density ρ_i of 916.8 kg m^{-3} so the mass m_i of ice
517 has a volume of $v_i = (m_i / \rho_i)$. The silicate volume is still v_s and so the final bulk density is β_f
518 where
519
520 $$\beta_f = (m_i + m_s) / (v_i + v_s) = (m_i + m_s) / [(m_i / \rho_i) + (m_s / \rho_s)] \quad (15).$$
521
522 Equation (12) gives (m_i / m_w) and equation (2) gives (m_w / m_s) so in terms of these,
523
524 $$\beta_f = [(m_i / m_w) + (m_w / m_s)^{-1}] / \{[(m_i / m_w) / \rho_i] + [\rho_s\ (m_w / m_s)]^{-1}\} \quad (16).$$
525
526 The density, ρ_s, of the clay minerals in the experimental mud was ~2500 kg m^{-3} and the bulk
527 density of the mud was ~1040 kg m^{-3}, implying that the clay component formed ~6.5 % of

the mud mass. The mud was released into ambient experimental chamber pressures in the range 650-700 Pa, and initial mud temperatures were up to ~275.5 K. Taking account of the weight of the overlying mud and the experimental chamber pressure, the saturation vapour pressure of water, with values up to ~730 Pa [48], would have been reached at depths up to 5-6 mm in the experiments. The relative values of the specific heat and the latent heat of evaporation of water are such that while the mud was cooling from ~275.5 K to its freezing point, ~0.34 % of its water would have been lost, having a trivially small effect on its essentially Newtonian rheology. By the time subsequent vapour loss had frozen the remaining water, ~88 % of the initial mass of water would have been converted to ice at the expense of losing ~12 % of the initial water mass as vapour, leaving solid mud with a density of ~961 kg m^{-3}, slightly less dense than the original liquid mud. This should have produced a frozen crust, again of thickness 5-6 mm, beneath which the mud would have been partially liquid, as observed in the experiments. In similar scale flows under martian gravity, the thermodynamics of this process would have been the same, as it involves only heat transfer by conduction, but the thickness of the frozen outer crust would have been greater, 14-17 mm, because the pressure in the mud depends on the acceleration due to gravity [49].

Data availability

The movies, photos, pressure and temperature logs generated during and analysed during the current study that support our findings are available in the Zenodo repository with the identifier DOI: 10.5281/zenodo.3457148 (https://doi.org/10.5281/zenodo.3457148).

References

[42] Platz, T., Byrne, P. K., Massironi, M. & Hiesinger, H. Volcanism and tectonism across the inner solar system: an overview. Geological Society, London, Special Publications 401, 1–56 (2014).

552 [43] Corradi, A. B., Manfredini T., Pellacani, G. C. & Pozzi, P. Deflocculation of Concentrated
553 Aqueous Clay Suspensions with Sodium Polymethacrylates. Journal of the American
554 Ceramic Society 77, 2, 509–513 (1994). https://doi.org/10.1111/j.1151-
555 2916.1994.tb07022.x

556 [44] Clark, B. C. Implications of abundant hygroscopic minerals in the martian regolith. Icarus
557 34, 645–665 (1978). https://doi.org/10.1016/0019-1035(78)90052-0

558 [45] Vaniman, D. T. et al. Magnesium sulphate salts and the history of water on Mars. Nature
559 431, 663–665 (2004). https://doi.org/10.1038/nature02973

560 [46] Hecht, M. H., et al. Detection of perchlorate and the soluble chemistry of martian soil at
561 the Phoenix lander site. Science 325, 64–67 (2009).
562 https://doi.org/10.1126/science.1172466

563 [47] Westoby, M. J., Brasington, J., Glasser, N. F., Hambrey, M. J. & Reynolds, J. M.
564 'Structure-from-motion' photogrammetry: a low-cost, effective tool for geoscience
565 applications. Geomorphology 179, 300–314 (2012).
566 https://doi.org/10.1016/j.geomorph.2012.08.021

567 [48] Lide, D. R. (ed.). CRC Handbook of Chemistry and Physics (85th edition, CRC Press,
568 Boca Raton, Florida, 2004).

569 [49] Pedersen, G. B. M. Frozen Martian lahars? Evaluation of morphology, degradation and
570 geologic development in the Utopia-Elysium transition zone. Planetary and Space
571 Science 85, 59–77 (2013). https://doi.org/10.1016/j.pss.2013.05.020


a
b
c

572

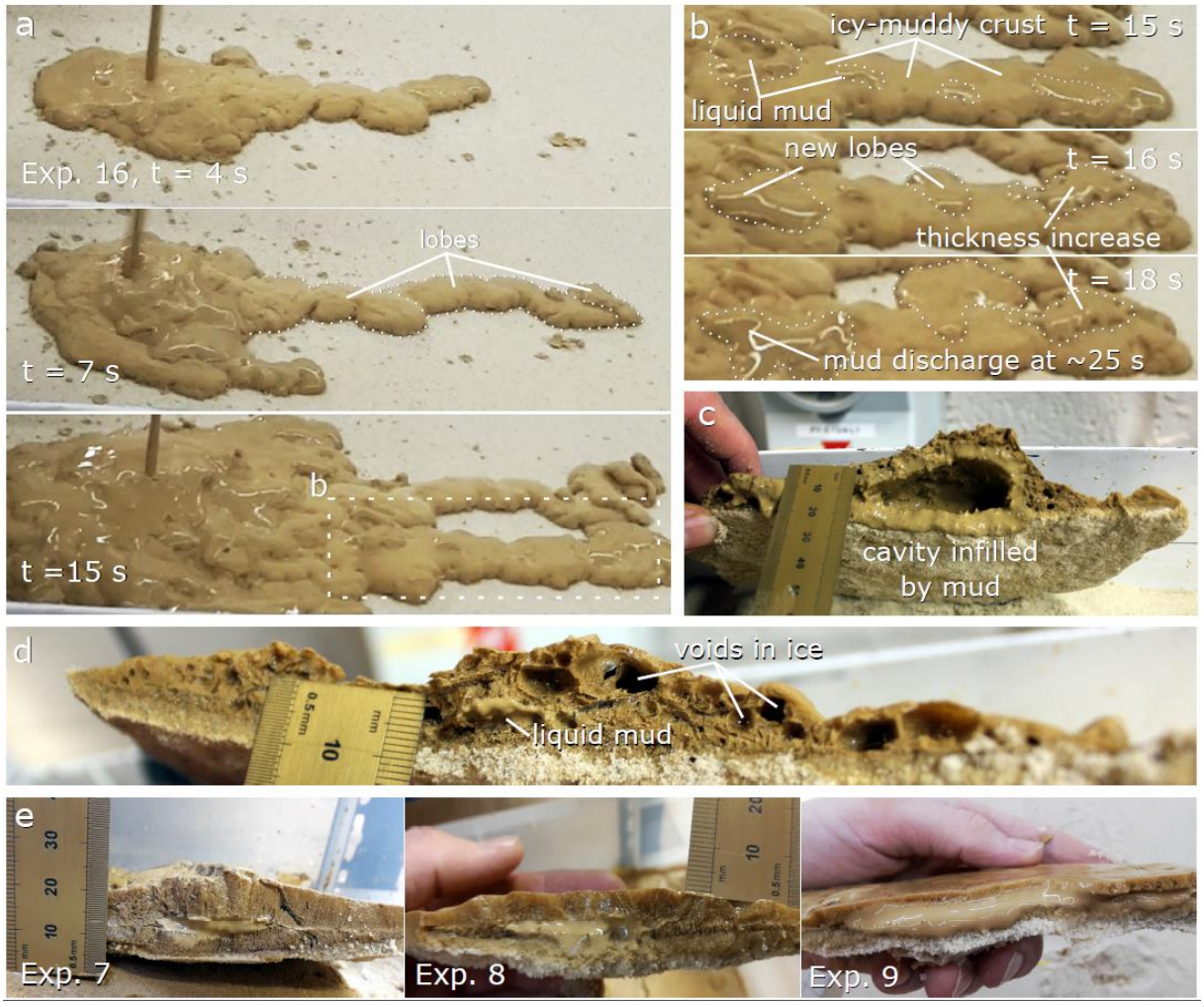
a
Exp. 16, t = 4 s
lobes
t = 7 s
b
t =15 s
b
icy-muddy crust t = 15 s
liquid mud
new lobes
t = 16 s
thickness increase
t = 18 s
mud discharge at ~25 s
c
cavity infilled
by mud
d
voids in ice
liquid mud
e
Exp. 7
Exp. 8
Exp. 9

573

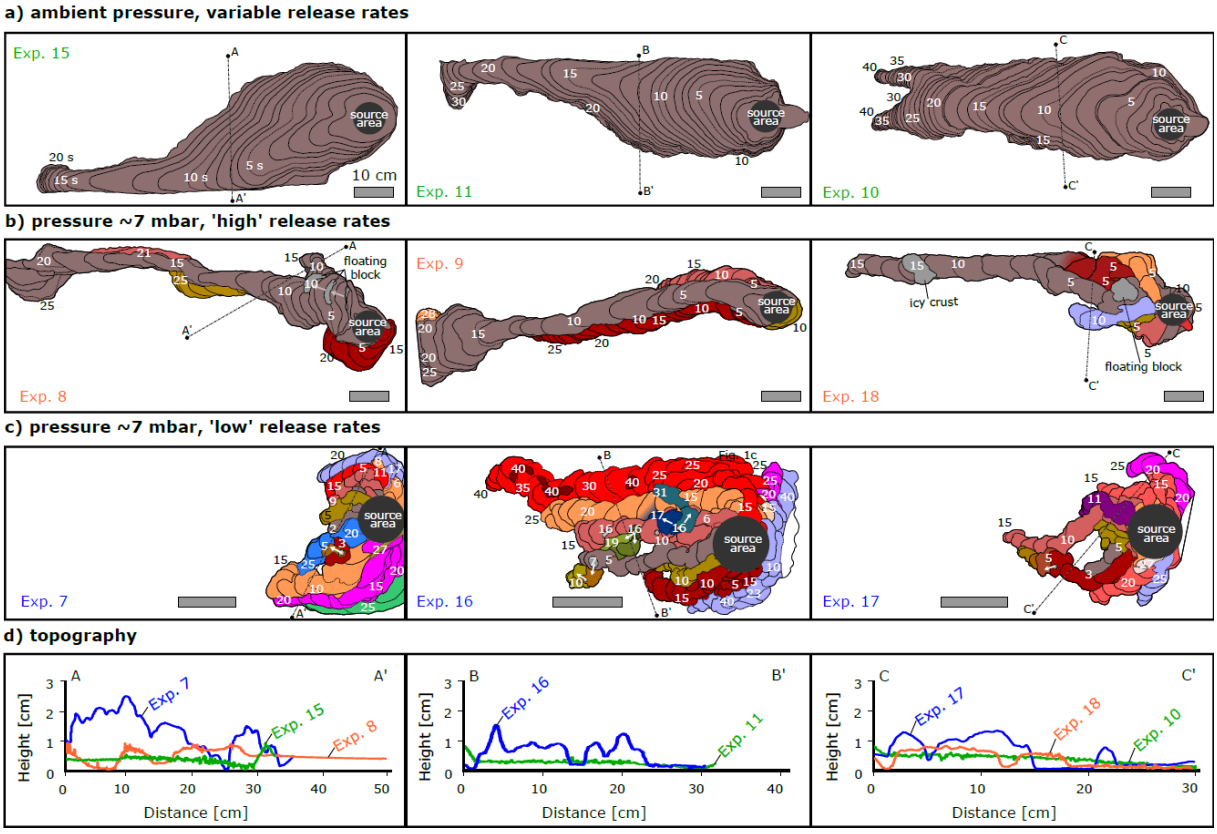
a) ambient pressure, variable release rates
Exp. 15
Exp. 11
Exp. 10
source area
20 s
15 s
10 s
5 s
10 cm
b) pressure ~7 mbar, 'high' release rates
Exp. 8
Exp. 9
Exp. 18
floating block
icy crust
c) pressure ~7 mbar, 'low' release rates
Exp. 7
Exp. 16
Exp. 17
d) topography
Exp. 7
Exp. 15
Exp. 8
Exp. 16
Exp. 11
Exp. 17
Exp. 18
Exp. 10
Height [cm]
Distance [cm]

574

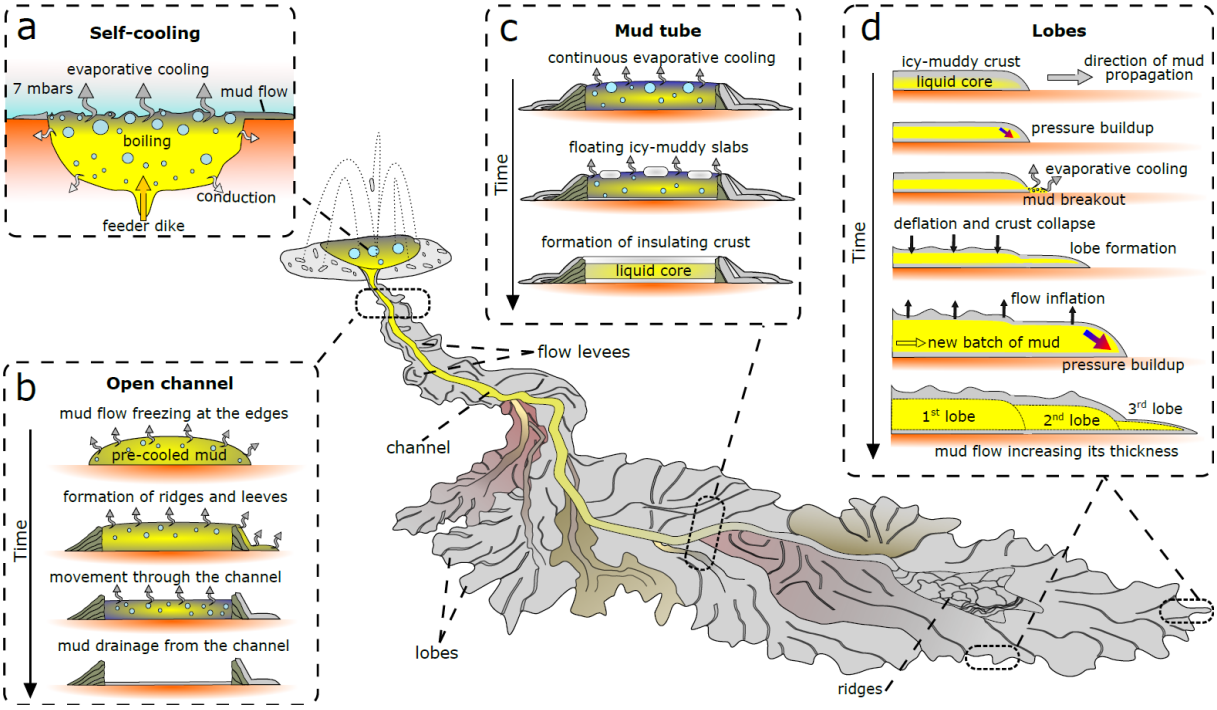
a
Self-cooling
evaporative cooling
7 mbars
mud flow
boiling
conduction
feeder dike
b
Open channel
mud flow freezing at the edges
pre-cooled mud
formation of ridges and leeves
movement through the channel
mud drainage from the channel
Time
c
Mud tube
continuous evaporative cooling
floating icy-muddy slabs
formation of insulating crust
liquid core
Time
d
Lobes
icy-muddy crust
liquid core
direction of mud propagation
pressure buildup
evaporative cooling
mud breakout
deflation and crust collapse
lobe formation
flow inflation
new batch of mud
pressure buildup
1st lobe
2nd lobe
3rd lobe
mud flow increasing its thickness
Time
flow levees
channel
lobes
ridges

575

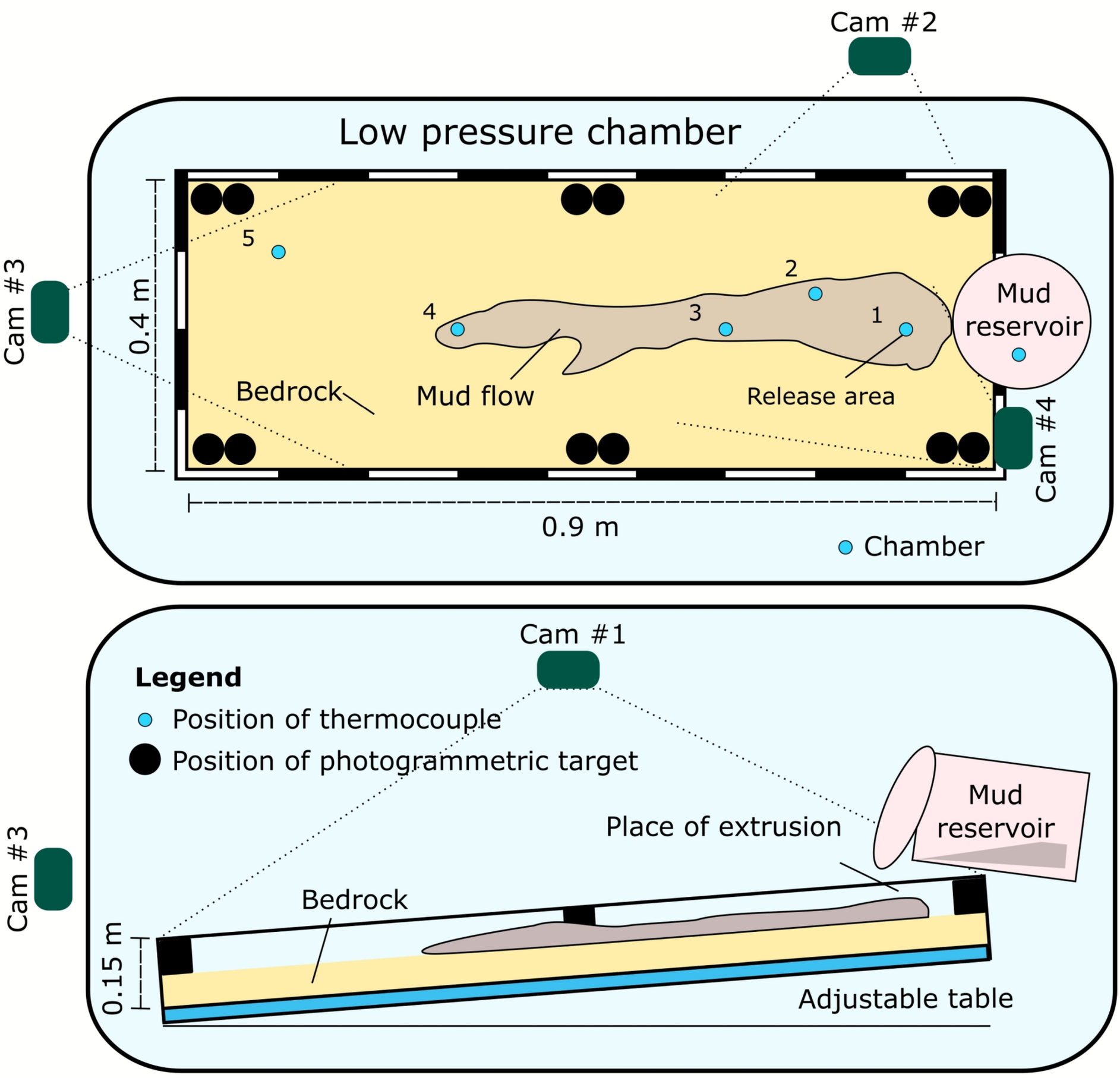
Cam #2
Low pressure chamber
Cam #3
0.4 m
5
4
3
2
1
Mud reservoir
Bedrock
Mud flow
Release area
Cam #4
0.9 m
Chamber
Cam #1
Legend
Position of thermocouple
Position of photogrammetric target
Cam #3
Place of extrusion
Mud reservoir
Bedrock
0.15 m
Adjustable table

Exp #	Pressure range [mbar]	Inclination [°]	Release time* [s]	Surface T** [°K]	Mud T*** [°K]	Type of surface	Salinity****
5	6.55 - 7.33	5	15	265	294	sand	D.I. water
6	7.16 - 7.66	5	26	264	292	sand	tap water
7	6.43 - 7.02	5	27	258	296	sand	saline water
8	7.11 - 7.37	5	25	261	294	sand	saline water
9	7.09 - 7.63	5	27	262	294	sand	saline water
10	1000	5	21	258	290	sand	saline water
11	1000	5	19	264	274	sand	saline water
15	1000	5	15	258	293	sand	saline water
16	6.32 - 6.54	5	46	256	290	sand	saline water
17	6.57 - 6.94	5	34	252	278	sand	saline water
18	6.37 - 6.58	5	15	260	290	sand	saline water
19	6.06 - 6.81	10	35	258	286	sand	saline water
21	6.55 - 6.77	10	34	253	293	sand	saline water
22	7.08 - 7.36	10	37	254	294	sand	saline water
23	6.43 - 6.97	5	40	265	293	plastic plate	saline water
24	6.66 - 7.11	5	28	254	295	plastic plate	saline water
29	6.55 - 7.08	5	40	259	295	plastic plate	saline water
34	5.29 - 6.55	5	failed exp.	259	297	plastic plate	saline water
41	1000	5	42	244	295	plastic plate	saline water
49	1000	5	34	247	290	plastic plate	saline water
54	1000	5	34	249	277	plastic plate	saline water

* Time period over which the mud was poured from the container

** Temperature of the surface before the release of the mud from the flipping container

*** Temperature of the mud within the container before the pressure drop

**** Saline water refers to a mixture of water that contains 0.5% w/w dissolved magnesium sulphate ($MgSO_4$)